



Anais da Academia Brasileira de Ciências

ISSN: 0001-3765

aabc@abc.org.br

Academia Brasileira de Ciências

Brasil

SCHMAL, MARTIN; FREUND, HANS-JOACHIM

Towards an atomic level understanding of niobia based catalysts and catalysis by combining the science of catalysis with surface science

Anais da Academia Brasileira de Ciências, vol. 81, núm. 2, junio, 2009, pp. 297-318

Academia Brasileira de Ciências

Rio de Janeiro, Brasil

Available in: <http://www.redalyc.org/articulo.oa?id=32713477016>

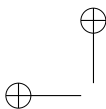
- How to cite
- Complete issue
- More information about this article
- Journal's homepage in redalyc.org

redalyc.org

Scientific Information System

Network of Scientific Journals from Latin America, the Caribbean, Spain and Portugal

Non-profit academic project, developed under the open access initiative



Anais da Academia Brasileira de Ciências (2009) 81(2): 297-318
(Annals of the Brazilian Academy of Sciences)
ISSN 0001-3765
www.scielo.br/aabc

Towards an atomic level understanding of niobia based catalysts and catalysis by combining the science of catalysis with surface science

MARTIN SCHMAL¹ and HANS-JOACHIM FREUND²

¹NUCAT PEQ Coppe/UFRJ, Centro de Tecnologia, Bl. G, Sala 128, Cidade Universitária, 21945-970 Rio de Janeiro, RJ, Brasil

²Fritz-Haber-Institut der Max-Planck-Gesellschaft, Department of Chemical Physics
Faradayweg 4-6, D-14195 Berlin, Germany

*Manuscript received on November 18, 2008; accepted for publication on March 4, 2009;
contributed by MARTIN SCHMAL* and HANS-JOACHIM FREUND**

ABSTRACT

The science of catalysis and surface science have developed, independently, key information for understanding catalytic processes. One might argue: is there anything fundamental to be discovered through the interplay between catalysis and surface science?

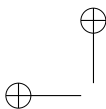
Real catalysts of monometallic and bimetallic Co/Nb₂O₅ and Pd-Co/Nb₂O₅ catalysts showed interesting selectivity results on the Fischer-Tropsch synthesis (Noronha et al. 1996, Rosenir et al. 1993). The presence of a noble metal increased the C₅⁺ selectivity and decreased the methane formation depending of the reduction temperature. Model catalyst of Co-Pd supported on niobia and alumina were prepared and characterized at the atomic level, thus forming the basis for a comparison with “real” support materials. Growth, morphology and structure of both pure metal and alloy particles were studied. It is possible to support the strong metal support interaction suggested by studies on real catalysts via the investigation of model systems for niobia in comparison to alumina support in which this effect does not occur. Formation of Co²⁺ penetration into the niobia lattice was suggested on the basis of powder studies and can be fully supported on the basis of model studies. It is shown for both real catalysts and model systems that oxidation state of Co plays a key role in controlling the reactivity in Fischer-Tropsch reactions systems and that the addition of Pd is a determining factor for the stability of the catalyst. It is demonstrated that the interaction with unsaturated hydrocarbons depends strongly on the state of oxidation.

Key words: catalysis, model catalysts, cobalt, palladium, characterization, niobia.

INTRODUCTION

The science of catalysis and surface science have developed over the years in friendly contact, though to a large extent independently. There are, however, examples in which key information for our understanding of catalytic processes has been gained from studies in surface science, one example being ammonia synthesis (Schlögl 2008). The science of surface science has been

that nitrogen is hydrogenated after N₂ dissociation on the surface was honored with the 2007 Nobel Prize (Gerhard Ertl (Ertl 2008)). Even though ammonia synthesis is a special case, one might argue: does this mean all fundamental problems in catalysis have been solved or putting it in another way: is there anything fundamental to be discovered through this interplay between catalysis and surface science?



ing the complex materials active as catalysts and those connected with operating conditions.

Complexity often does not only lead to qualitative changes but to new phenomena that do not occur in simpler systems. They need to be understood to be able to describe catalytic phenomena reliably.

Natural gas is becoming more attractive as an energy source due to the increasing prices of oil, the huge reserves of gas and environmental issues (Noronha et al. 2000a, Nowak Ziolk 1999, Passos et al. 2000, Schmal et al. 2000, Tanabe 2003, Wachs 2005, Ziolk 2003). This has led researchers across the globe to develop more economic processes of upgrading natural gas to higher hydrocarbon fuel. The Fischer-Tropsch synthesis is an alternative route to produce liquid fuels from synthetic gas.

Monometallic cobalt catalysts are known to be effective for the synthesis of long chain hydrocarbons from hydrogen and carbon monoxide (Anderson 1984, Dry 1981). The catalytic hydrogenation (activity, selectivity and stability) of carbon monoxide on cobalt catalysts has been reported to be affected by two factors: the dispersion and the extent of reduction (Fu and Bartholomew 1985, Ho et al. 1990, Lee et al. 1988, Reuel and Bartholomew 1984). The reducibility of cobalt is closely related to the nature of the species present on the support. In particular, on supported cobalt catalysts, several cobalt species have been detected as a function of the support (Arnoldy and Moulijn 1985, Castner and Santilli 1984, Ho et al. 1992, Lapidus et al. 1991, Noronha et al. 1999, Sato et al. 1984). At least three different types of cobalt species have been reported on the alumina-supported cobalt catalysts: Co_3O_4 particles, which are more readily reduced, Co^{2+} species and CoAl_2O_4 , which are hardly reduced or unreduced, respectively (Castner and Santilli 1984, Chin and Hercules 1982, Stranick et al. 1987, Tung et al. 1990). Analysis revealed that catalysts with low cobalt content showed a high amount of Co^{2+} species in interaction with the support. For higher cobalt loading, Co_3O_4 particles were also present, in addition to Co^{2+} species (Höbel et al. 2006).

al. 1991, Kapoor et al. 1992, Niemantsverdriet et al. 1988, Schanke et al. 1995, Zsoldos et al. 1991). Generally, it has been proposed that the addition of a noble metal promotes cobalt oxide reduction (Idriss et al. 1992, Juszczak et al. 1993, Kapoor et al. 1992, Martens et al. 1986, Sarkany et al. 1995, Schanke et al. 1995, Van'T Blik and Prins 1986).

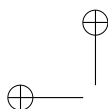
The addition of a noble metal to $\text{Co}/\text{Nb}_2\text{O}_5$ catalysts showed interesting selectivity results on the Fischer-Tropsch synthesis (Noronha et al. 1996, Rosenir et al. 1993). The presence of a noble metal increased the C_5^+ selectivity and decreased the methane formation independent of the reduction temperature. However, the characterization of the reduced state was not performed, rendering a complete comprehension of the catalytic behavior difficult.

In fact, relatively few studies have been performed to study the behavior of bimetallic systems on a support able to promote the Strong Metal Support Interaction (SMSI) effect, such as Nb_2O_5 (Ahon et al. 2006, Noronha et al. 2000b). This may be explained by the difficulties in characterizing the niobium oxide supported catalysts.

Some questions in those contexts have been addressed and there are several review articles available. We review here a joint venture between the catalysis groups in Rio de Janeiro and the surface science groups in the Fritz Haber Institute that was triggered by the Brazilian group in trying to understand Fischer-Tropsch catalysis on cobalt based alloy systems, in which particles on a variety of oxidic supports, such as alumina and niobia, just to mention two of them, have been studied.

Based on the experimental results of the group in Rio, the following questions were posed to the surface scientists:

1. Is it possible to prepare model Pd-Co alloys systems on the supports in question?
2. Is it possible to measure properties and reactivities of those model systems that may be compared to the “real” catalysts?



NIOBIA BASED REAL CATALYSTS AND MODEL SYSTEMS

venture and try to address some of the fundamental questions that one encounters on such a journey (Carlsson et al. 2003a, b, c, Freund et al. 2003, Heemeier et al. 2002, Hill et al. 2005, Höbel et al. 2006, Mendes et al. 2006a, b, Nowitzki et al. 2007, Risse et al. 2004, Starr et al. 2005, Uhl et al. 2007).

EXPERIMENTAL

The real carriers were prepared from commercial materials by simple calcination in air. Niobium oxide with a specific surface area of $30 \text{ m}^2\text{g}^{-1}$ was obtained after calcination at 873 K of the hydrated oxide (sample AD 376 from *Companhia Brasileira de Metalurgia e Mineração*). Alumina was obtained from a transition alumina (sample 3996-R, area $200 \text{ m}^2\text{g}^{-1}$, from Harshaw) by treatment at 1473 K. The catalysts were prepared by impregnation with an aqueous solution of cobalt nitrate. The impregnated material was dried in air at 383 K for 16 h and then calcined in flowing air at 673 K for 16 h. The metal loading was always 5 wt.%. The specific surface areas of the calcined samples were $23 \text{ m}^2\text{g}^{-1}$ (Co/Nb₂O₅) and $9 \text{ m}^2\text{g}^{-1}$ (Co/Al₂O₃) (Rosenir et al. 1993).

The bimetallic catalyst was prepared on the same support by incipient wetness impregnation or co-impregnation of the support with an aqueous solution of palladium nitrate and cobalt nitrate, followed by drying at 393 K for 16 h and calcination in air at 673 K for 2 h. Table I lists the catalysts and their metal contents, measured by atomic absorption spectroscopy (Noronha et al. 2000b).

TABLE I
Composition of bimetallic catalysts
(Noronha et al. 2000b).

Catalyst	Composition (wt.-%)	
	Pd	Co
Pd/Nb ₂ O ₅	1.3	—
Pd ₃₅ Co ₆₅ /Nb ₂ O ₅	2.1	2.1
Pd ₁₅ Co ₈₅ /Nb ₂ O ₅	1.6	5.0
Co/Nb ₂ O ₅	—	2.0

On the other hand, for the model catalyst, an as-

scription is found within the website of the Fritz Institute (<http://www.fhi-berlin.mpg.de/>).

RESULTS

REAL CATALYSTS

Activation

Figure 1 presents the Temperature Programmed Reduction (TPR) profiles for some typical catalysts. In all cases, the reduction occurs, at least, in two distinct steps, whose resolution depends on the sample and/or the carrier. Pure Co₃O₄ and the mechanical mixture of Co₃O₄ and Nb₂O₅ are much easier to reduce than the supported catalysts. The experimental ratio H₂:Co, also given in Figure 1, is close to the theoretical value (1.33) for the supported materials and for Co/Al₂O₃, but is much higher for Co/Nb₂O₅, suggesting a partial reduction of the carrier.

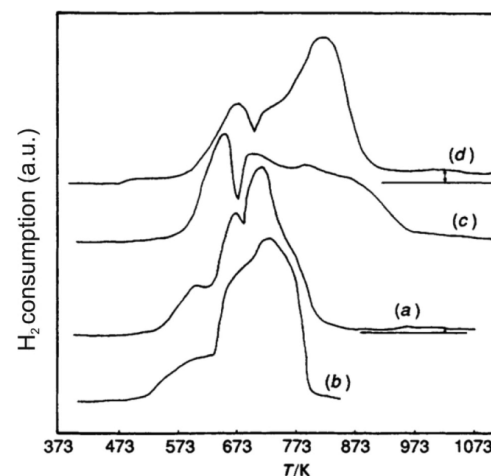


Fig. 1 – TPR profiles for (a) physical mixture ($\text{H}_2:\text{Co} = 1.33$); (b) $\text{Co}_{23}\text{O}_{34}$ ($\text{H}_2:\text{Co} = 1.30$); (c) $\text{Co}/\text{Al}_2\text{O}_3$ ($\text{H}_2:\text{Co} = 1.33$); (d) $\text{Co}/\text{Nb}_2\text{O}_5$ ($\text{H}_2:\text{CO} = 1.49$) (Rosenir et al. 1993).

The results of hydrogen and oxygen chemisorption for Co/Nb₂O₅ and Co/Al₂O₃, for different reduction temperatures, are given in Table II. The oxygen uptake on the pure niobia carrier, reduced at various temperatures, and the O₂:H ratios are also shown.

For Co/Al₂O₃ catalysts, the hydrogen uptake is dependent of the temperature of reduction, both

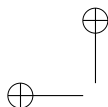


TABLE II
H₂ and O₂ adsorption for different reduction temperatures (Rosenir et al. 1993).

gas uptake/ μmol						
Co/support Nb ₂ O ₅						
catalyst	red. temp./K	H ₂	O ₂	O ₂	O:H	R ^a (%)
Co/Al ₂ O ₃	573	34.9	—	—	—	—
Co/Al ₂ O ₃	773	34.6	—	—	—	—
procedure 1						
Co/Nb ₂ O ₅	533	54.3	—	—	—	—
Co/Nb ₂ O ₅	573	28.9	59.5	0.4	2.4 (2.0)	89
Co/Nb ₂ O ₅	673	13.4	58.5	6.3	4.4 (3.9)	—
Co/Nb ₂ O ₅	773	5.3	59.7	13.5	11.3 (8.7)	94
procedure 2						
Co/Nb ₂ O ₅	573	31.5	111.2	—	3.5 (3.1)	—
Co/Nb ₂ O ₅	773	7.1	109.5	—	15.4 (13.5)	—

M = 2g; values in parentheses discounting O₂ due to the adsorption on pure Nb₂O₅. ^aFrom magnetic measurements.

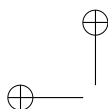
TABLE III
Estimation of dispersion and particle sizes of catalysts. The dispersions and the particle sizes were calculated assuming that the degree of the reduction, for both temperatures, is ca. 100% with cobalt loading of 4.49 wt.% for Co/Nb₂O₅ and 4.5 wt.% for Co/Al₂O₃. The dispersions and the particles sizes were calculated assuming the nominal cobalt loading (5 wt.% Co) and the degree of reduction obtained from magnetic measurements. Values measured according to procedure 2 (Rosenir et al. 1993).

catalyst	red. temp./K	dispersion ^a (%)			d _p /nm ^a	
Co/Al ₂ O ₃	573	4.6		21.8		
	773	4.5		22.0		
Co/Nb ₂ O ₅	533	7.1		14.0		
	573	3.8	3.8 ^b	26.3	26.0 ^b	26.8 ^c
	663	1.8		56.6		
	773	1.0	0.9 ^b	104.0	109.5 ^b	119 ^c

unchanged. In a second procedure, the hydrogen uptake is similar to that obtained from direct reduction, at the same temperatures. In this case, although independent of the temperature of reduction, the oxygen uptake is increased by a factor of 2. This is not yet well explained and needs further investigation. The O₂:H ratio increases with the temperature of reduction, in both cases. The re-

From hydrogen chemisorption measurements, the apparent cobalt dispersion and cobalt mean particle size were calculated, with the hypothesis that the H:Co surface stoichiometry is 1. The results are given in Table III. Note that the particle size is similar for both Co/Nb₂O₅ and Co/Al₂O₃ reduced at 573 K.

The reduction profiles of the bimetallic Pd-Co cat-



NIOBIA BASED REAL CATALYSTS AND MODEL SYSTEMS

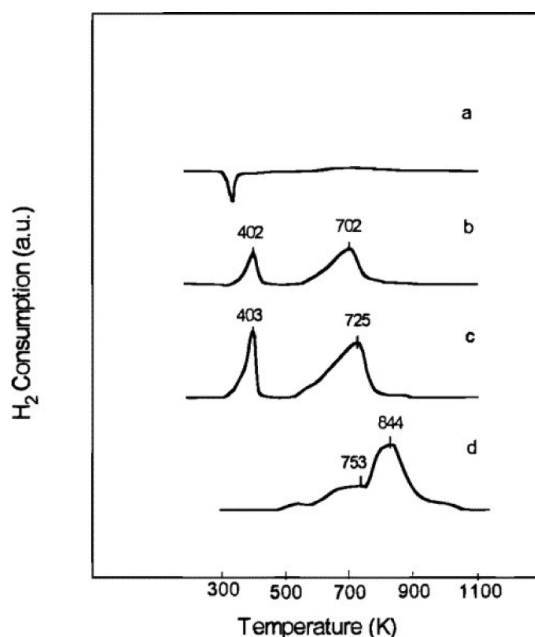


Fig. 2 – Reduction profiles of the niobia-supported catalysts. (a) Pd/Nb₂O₅; (b) Pd₃₅Co₆₅/Nb₂O₅; (c) Pd₁₅Co₈₅/Nb₂O₅; (d) Co/Nb₂O₅ (Noronha et al. 2000b).

et al. 2000b). The bimetallic catalysts showed peaks at temperatures around 400 and 700 K. The hydrogen consumption at room temperature (Table IV) was higher than the theoretical value expected for complete reduction of PdO, indicating that, besides PdO reduction, another process may occur. As PdO was completely reduced at room temperature, the peaks at 400 and 700 K can be ascribed to the reduction of cobalt oxides. However, these maxima were shifted toward lower temperatures, compared to the cobalt reduction of the monometallic Co/Nb₂O₅ catalyst, indicating that palladium catalyzes the cobalt oxide reduction.

Therefore, the palladium addition promoted not only the reduction of Co₃O₄ particles but also that of the cobalt surface phase. The magnetic measurements coupled with TPR analyses will allow us to quantify this promotional effect. Saturation of magnetization was determined from the magnetization curves for each sample reduced at increasing temperatures, and the reduction degree of cobalt was calculated (Table V).

of cobalt in metallic state, which was much lower than that calculated from the hydrogen uptake during the reduction. As it was discussed for the Pd/Nb₂O₅ catalyst, this difference could be attributed to a partial reduction of cobalt at high temperature.

The magnetic measurements of the Pd₃₅Co₆₅/Nb₂O₅ bimetallic catalyst showed the presence of metallic cobalt even after reduction at room temperature, confirming a strong promoting effect of palladium on cobalt oxide reduction. After reduction at 473 K, magnetic measurements indicated that 12% of cobalt was already in the metallic state (Table V). However, the hydrogen consumption measured by TPR (Table IV) was higher than the amount of metallic cobalt produced, suggesting a partial transformation of Co₃O₄ to Co⁰ in this temperature range as well. The reduction at 873 K led to a complete reduction of cobalt oxides, in agreement with the behavior observed on the Co/Nb₂O₅ catalyst. This result indicated that palladium also promotes the reduction of the Co²⁺ species since X-ray Photoelectron Spectroscopy (XPS) and TPR analysis revealed the presence of a cobalt surface phase. Thus, the magnetic measurements performed at different reduction temperatures support the TPR results, giving a further evidence of the interaction between both metals.

In the case of Pd₁₅Co₈₅/Nb₂O₅ bimetallic catalyst, after reduction at room temperature, the magnetic measurements did not suggest the presence of metallic cobalt. After reduction at 473 K, the amount of metallic cobalt was lower than on Pd₃₅Co₆₅/Nb₂O₅ catalyst. In other words, the promoting effect of palladium decreases with the increase of cobalt loading. However, after reduction at 873 K, all cobalt oxide was reduced to the metallic state, as observed for the Pd₃₅Co₆₅/Nb₂O₅ catalyst.

Catalytic results

The catalytic results are summarized in Table VI. The reaction rates for Co/Al₂O₃ are equal and independent of the temperature of reduction. However, when the temperature of reduction is increased from 533 to 773 K, the reaction rate with Co/Nb₂O₅ is reduced by a factor of 10.

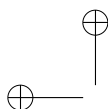


TABLE IV
TPR hydrogen uptakes for bimetallic catalysts (Noronha et al. 2000b).

Catalyst	Experimental			Theoretical ^a	
	T _{amb}	298–473 K	473–873 K	Pd	Co
Pd/Nb ₂ O ₅	10.8	–1.4	1.4	9.4	—
Pd ₃₅ Co ₆₅ /Nb ₂ O ₅	6.4	2.0	6.5	4.7	11.4
Pd ₁₅ Co ₈₅ /Nb ₂ O ₅	4.1	4.8	12.8	2.3	17.2
Co/Nb ₂ O ₅	—	—	18.4	—	22.6

^aTheoretical H₂ uptake corresponds to the following reactions: Pd T_{amb}:PdO → Pd⁰; Co 298–473 K:Co₃O₄ → CoO; Co 473–873 K:CoO → Co⁰; Co Co²⁺ → Co⁰.

TABLE V
Magnetic measurements of reduced bimetallic catalysts (Noronha et al. 2000b).

Catalyst	Metallic Co (%)		
	T _{room}	298–473 K	473–873 K
Pd/Nb ₂ O ₅	a	a	a
Pd ₃₅ Co ₆₅ /Nb ₂ O ₅	4	12	105
Pd ₁₅ Co ₈₅ /Nb ₂ O ₅	a	4	105
Co/Nb ₂ O ₅	a	a	43

^aPresented only a diamagnetic signal.

TABLE VI
Influence of the reduction temperature (K) on activity and selectivity (Rosenir et al. 1993).

Catalyst	red. temp./K	mass/g	conv. ^a (%)	TOF/10 ^{–3}			S (%)			
				rate(CO) ^b	CO ^c	C ₁ ^c	CH ₄	C ₂ –C ₄	C ₅ ⁺	CO ₂
Co/Nb ₂ O ₅	533	0.8	10.1	7.41	27	17	62.5	24.6	10.3	2.6
Co/ Nb ₂ O ₅	573	0.8	9.7	6.45	45	23	52.3	29.3	16.1	2.3
Co/ Al ₂ O ₃	573	1.5	16.9	6.6	38	21	54.5	24.1	12.8	8.5
Co/ Nb ₂ O ₅	673	2.0	10.6	3.2	48	8.1	17.0	33.3	34.8	2.2
Co/ Nb ₂ O ₅	773	4.0	8.2	1.13	43	6.6	14.1	34.8	48.8	2.3
Co/ Al ₂ O ₃	773	1.5	16.5	6.1	35	20	56.2	23.6	11.4	8.8

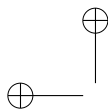
H₂/CO = 2, P = 1 atm, T_{reaction} = 533 K. ^aAfter 24 h. ^b10^{–7} mol s^{–1} g_{cat}^{–1}. ^cBased on H₂ uptake on fresh sample (s^{–1}).
^d $S_{C_n H_x} = \frac{100nF_{C_n H_x}}{F_{CO_{in}} - F_{CO_{out}}}$; where $F_{C_n H_x}$ is the molar flow rate of species $C_n H_x$; $S_{C_n H_x} = 1 - \sum_{n=1}^4 S_{C_n H_x} - S_{CO_2}$.

for CO conversion for both Co/Al₂O₃ and Co/Nb₂O₅ is approximately constant.

While the selectivities (S) for C₁ and C₅⁺ with Co/Al₂O₃, at steady state, do not change, whatever the reduction temperature, the selectivities for C₁ and C₅⁺, with Co/Nb₂O₅, change drastically with increasing reduction

of variation in the degree of reduction, of poisoning and of sintering, our results can be analyzed in terms of the SMSI, progressively established for Co/Nb₂O₅ when the temperature of reduction is increased from 533 to 773 K.

The remaining SMSI state in Co/Nb₂O₅ catalysts induces a drastic reduction in methane formation and



NIOBIA BASED REAL CATALYSTS AND MODEL SYSTEMS

Figure 4 displays the selectivity with time on stream, for a space velocity of 6000h^{-1} and isoconversion (30%) for the Pd-Co catalysts, reaction temperature of 270°C and pressure of 20 bar, after reduction at 500°C . The bar diagrams of Figure 4a present product selectivities on $\text{Co}/\text{Nb}_2\text{O}_5$ catalyst based on moles of product carbons in the $C_{i,\text{range}}/\Sigma C_i$ formation with time on stream. Methane was very low ($\approx 3.0\%$) and the diesel fraction (C_{13-18}) was very high (54–49%). Note that CH_4 , C_{2-4} , C_{5-12} , C_{13-18} , and C_{19+} correspond to saturated hydrocarbons with the carbon subscript being the number of carbon atoms in the chain. The range C_{2-4} may also contain some C_{2-4} olefins (ethene and propene) which were not resolved from the more pronounced saturated hydrocarbon chromatographic peaks. Higher molecular weight olefins (C_{5-12} and C_{13-18}) were detected on the $\text{Co}/\text{Nb}_2\text{O}_5$ catalyst.

The bar diagrams of Figure 4b clearly point out that the selectivity towards methane and C_{2-4} hydrocarbons for the bimetallic $\text{Co-Pd}/\text{Nb}_2\text{O}_5$ changed with Pd addition and with time on stream. Note that the methane formation rate of this catalyst increased. Olefins, except $C_4^=$, were not detected before on the pure Co-containing catalysts. Light products and gasoline fractions increased, while diesel fraction decreased.

Methane was around 17–21% and the diesel fraction decreased from 53 to 37%. The addition of the second metal indicates also higher selectivity towards alkanes. Product retention and condensation are not expected to have occurred because the overall mass balance indicates that the reactor operates steady-state.

The stability of the bimetallic $\text{Pd-Co}/\text{Nb}_2\text{O}_5$ catalyst is shown in Figure 5 indicating good stability up to 50 h with time on stream for a reduction temperature of 500°C . It suggests that the Pd stabilizes the catalyst for a long time and from the beginning.

It is noteworthy, that the catalyst was stable during 50 hours and deviation of mass balance was around 20%. In addition, during the stabilization, samples after 50 h were taken and coke was analyzed by Thermogravimetry (TG) (not shown). It displays the loss of approximately 16% of carbon due to the coke deposition, which al-

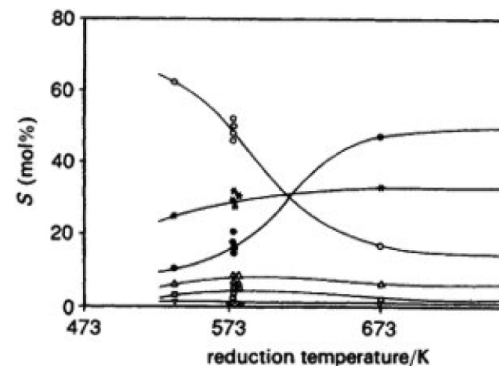


Fig. 3 – Influence of reduction temperature on selectivities Nb_2O_5 . \circ : S_{C_1} ; \square : S_{CO_2} ; ∇ : $S_{C_2=}$; Δ : S_{C_2} ; $*$: S_{C_2-} ; \diamond : $S_{C_5+} + O$; $\text{H}_2/\text{CO} = 2$, $P = 1 \text{ atm}$, $T_{\text{reaction}} = 533 \text{ K}$ (Rose 1993).

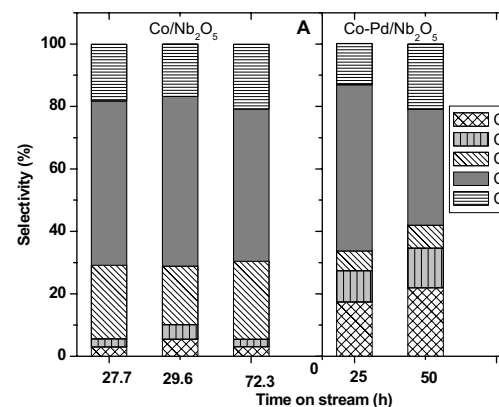
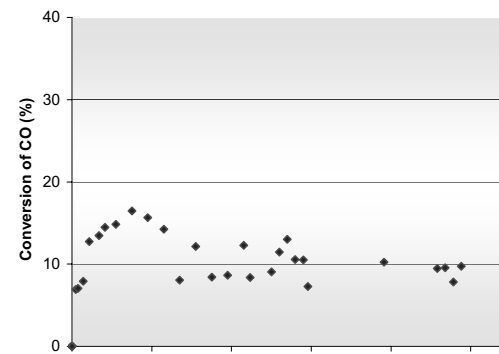
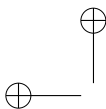


Fig. 4 – Catalytic test – $\text{H}_2/\text{CO} = 2$, 270°C , 20 atm, (A) $\text{Co}/\text{Nb}_2\text{O}_5$, (B) $\text{Co-Pd}/\text{Nb}_2\text{O}_5$.





The Anderson-Schulz-Flory equation (ASF) with these experiments displayed great deviation in the C_{13} - C_{18} range (Fig. 6). As expected, the total hydrocarbon molar compositions cannot be interpreted as an ASF distribution. Although the C_2 - C_3 anomalies and the change of the chain growth probability in the range from C_3 to C_8 - C_{12} range may be explained by α -olefin readsorption with secondary chain propagation and the existence of two mechanisms for chain propagation, the increasing selectivity observed between C_8 - C_{12} for all experiments cannot be explained by these mechanisms (Ahon et al. 2006).

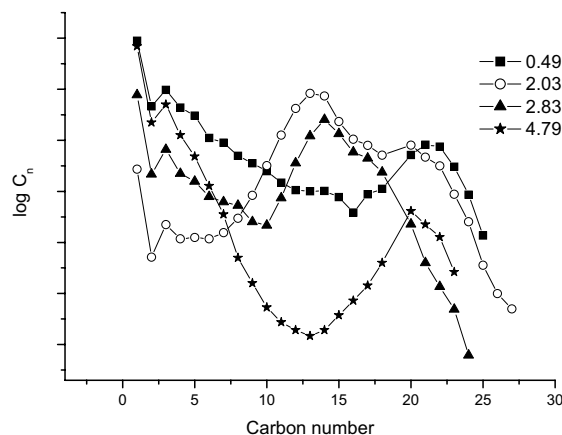


Fig. 6 – Anderson-Schulz-Flory of carbon distribution.

In conclusion, these results showed that more fundamental studies are needed to explain the behavior of a real catalyst, which was the objective to study a model catalyst, however, under UHV conditions.

MODEL STUDIES

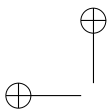
Modeling the technical support is a very difficult task and attempts to generate knowledge at the atomic level are being launched at present. This involves research at the liquid-solid interfaces (Catalano et al. 2008, Datta et al. 1992, Kim et al. 1993, Park et al. 2006, M. Sterrer, unpublished data).

So far, model oxide supports have been prepared under UHV conditions. One uses either conductive oxide single crystals or thin films grown on top of metal

und and Pacchioni 2008, Freund and Goodman 2007, Henry 1998, Risse et al. 2008). The supports relevant to the present review are alumina and niobia.

Alumina has been prepared by oxidation of a NiAl(110) single crystal (Jaeger et al. 1991, Libuda et al. 1994). Its structure and properties have been the object of intense studies across the world. Finally, Scanning Tunneling Microscopy (STM) (Kulawik et al. 2006) and Atomic Force Microscopy (AFM) (Simon et al. 2008) images with atomic resolution have been published, and density functional calculations (Kresse et al. 2005) have allowed us to understand the film at the atomic level including its defect structure, which turns out to be particularly relevant when it comes to anchoring of metal nanoparticles (Schmid et al. 2006). Figure 7 shows atomic resolution of STM and AFM images together with the structural model as deduced from Density Functional Theory (DFT) calculations at areas of the film that do not contain defects. It is possible to bind metal atoms within the unit cell, even without particular defects, but this depends critically on the possibilities of charge transfer through the layer and has only been found to occur for Au. Other metals, such as Pd, do not feel this effect and we have learned to understand this (Sterrer et al. 2007).

Niobia is difficult to prepare in a well-ordered fashion. Niehus and his group came up with a strategy to prepare Niobia on a $Cu_3Au(100)$ surface by predosing the surface with a “reactive” oxygen which dissolves in the alloy and then dosing Nb from a metal source which reacts with the predosed oxygen to form well-ordered niobia layers (Middeke et al. 2005). Figure 8 shows the morphology and structure of the film as imaged via STM (Starr et al. 2005). The large terraces (Fig. 8a) are separated by steps and those terraces exhibit one hexagonal atomic arrangement of oxygen atoms (Fig. 8b). The rotated domains are clearly discernable (Fig. 8c). It seems that this surface is not connected to any known surface terminations that could be deduced from known bulk structures. Understanding niobia has progressed lately but it seems that the surface structure depends on the thickness of the niobia film (Fig. 9). A thin film



NIOBIA BASED REAL CATALYSTS AND MODEL SYSTEMS

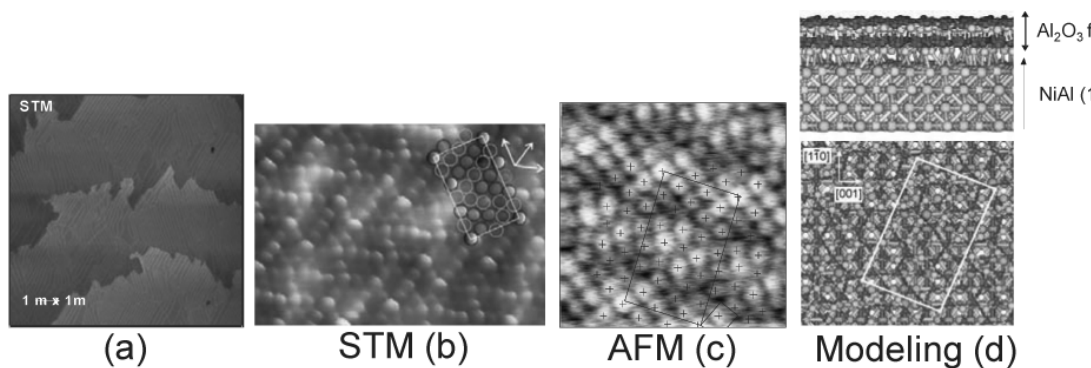


Fig. 7 – STM and AFM images of alumina on NiAl(110): (a) large scale STM image showing the antiphase domain boundaries, (b) high resolution STM, (c) atomic resolution AFM, (d) alumina as modeled with DFT top and side view (Kresse et al. 2005, Kulawik et al. 2008, et al. 2008).

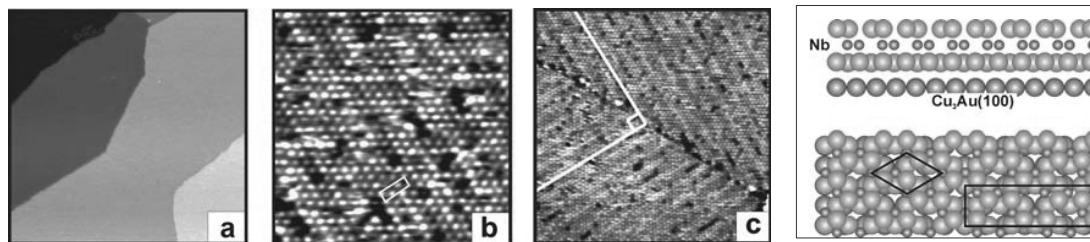
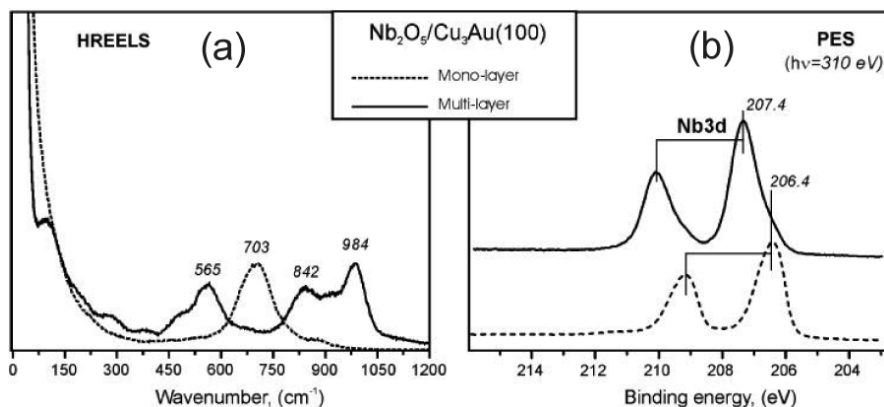
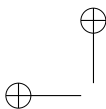


Fig. 8 – STM images of the niobia film grown on $\text{Cu}_3\text{Au}(100)$. (a) Large terraces separated by steps of $\sim 2\text{\AA}$ in height. (b) Hexagonal lattice of the niobia film with vacancy defects. The (2×7) superstructure cell is marked as a rectangle. (c) Two domains rotated by 90° , one domain exhibiting characteristic surface modulation seen as stripes. Image sizes and tunneling parameters are: (a) $200 \times 200\text{ nm}^2$, $\text{VS} = 1.0\text{ V}$, $I = 1.0\text{ nA}$; (b) $15 \times 15\text{ nm}^2$, $\text{VS} = 1.4\text{ V}$, $I = 1.0\text{ nA}$; (c) $40 \times 40\text{ nm}^2$, $\text{VS} = 1.4\text{ V}$, $I = 1.0\text{ nA}$. (d) Cross and top views of the niobia film grown on $\text{Cu}_3\text{Au}(100)$. The unit cell of niobia overlayer is indicated as a rhomb. The rectangle shows the (2×7) coincidence superstructure which is formed between oxide and metal substrate lattices. The surface shows a hexagonal lattice with a 5.3\AA periodicity (Mendes et al. 2005, Starr et al. 2005).





Nb=O double bonds (Fig. 9). The absence of any Nb=O double bonds is clear from High Resolution Electron Energy Loss Spectroscopy (HREELS) measurements, showing no significant intensity above $\sim 900\text{ cm}^{-1}$ (Fig. 9a).

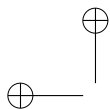
If one grows thicker films, one approaches the structures expected from bulk $\text{H-Nb}_2\text{O}_5$ (Fig. 9a) surfaces. In particular, niobyl species (Nb=O) are observed and the oxidation state is represented by a Nb3d XPS spectrum at the appropriate binding energy comparable to $\text{H-Nb}_2\text{O}_5$, while the monolayer is shifted to smaller (Fig. 9b) binding energy due to screening by the metallic substrate. Unfortunately, the multilayer exhibits some roughness. Figure 10a shows Infrared Reflection Absorption Spectroscopy (IRAS) spectra of CO adsorbed at 100 K after thermal flash to the specified temperatures and cooling back to 100 K. CO species with the stretching frequency of ~ 2190 and 2168 cm^{-1} have desorbed at 140 K, which correlates well with the TPD peak at 125 K. The same results are obtained by non-linear optical spectroscopy, i.e. sum frequency generation, which allows one to also go to higher pressures. Heating to 200 K results only in small increase of the peak intensity at 2141 cm^{-1} , indicating that CO species resulted in the TPD (Temperature Programmed Desorption) peak at 155 K are IR inactive. The most prominent peak at 2141 cm^{-1} disappears only upon further heating to 300 K, thus indicating that these species are associated with CO TPD signal at 272 K.

It is important to note that the integrated TPD area of CO desorbing from the niobia films is about five times smaller (Fig. 10b), on average, than from the clean $\text{Cu}_3\text{Au}(100)$ surface. Since the CO saturation coverage on $\text{Cu}_3\text{Au}(100)$ at 100 K is about 0.3 ML (Graham 1987), the amounts of CO adsorbed on the niobia surface is calculated to be less than 0.2 molecules per Nb_2O_5 unit cell (see Fig. 8d). On the other hand, as mentioned above, the CO coverage dependence (Fig. 10c) of the IRAS spectra in the $2141\text{--}2123\text{ cm}^{-1}$ range (see Fig. 8) indicates a strong CO-CO interaction. Bearing in mind that the thin niobia film is oxygen terminated as shown in Figure 8d, it appears that CO does

strong CO-CO interaction at the ill-defined boundaries between niobia domains, as observed by STM (Davydov 1984, Starr et al. 2005, Zecchina et al. 1996). Owing to the Pauli repulsion between carbon lone-pair electrons and the surface charge distribution, adsorbed CO seems to vibrate against a rigid wall (so called “wall effect”). As a result, the CO stretching frequency is shifted to higher wavenumbers compared to the gas phase value (2143 cm^{-1}). However, metal cations which contain partially filled d-orbitals can interact with the $2\pi^*$ -orbital of CO via electron back-donation from the metal to CO thus lowering the vibrational frequency (Blyholder 1964, Zecchina et al. 1996). On silica supported N_2O_5 particles, Knözinger and co-workers observed the signal at 2191 cm^{-1} (i.e. blueshifted with respect to CO in the gas phase) which was assigned to CO bonded to Nb^{5+} surface atoms (Beutel et al. 1997). Therefore, the weak signal at $2189\text{--}92\text{ cm}^{-1}$ observed on the niobia films can be assigned to the adsorption on the Nb^{5+} cations. Concomitantly, the most prominent peak at 2141 cm^{-1} can be associated with Nb species, which are partially reduced and thus contain d-electrons through which Nb interacts more strongly with CO via back-donation effect. For example, step edges of the niobia terraces and domain boundaries can in principle expose low coordinated and partially reduced Nb cations, which may adsorb CO much stronger than regular terrace sites.

Since, for the “real” catalysts, the niobia component was dispersed on an alumina support, the modeling procedure needs one more step, namely the preparation of alumina supported niobia. Those were prepared by physical vapor deposition of Nb in an oxygen atmosphere onto the above described thin alumina film.

Figure 11 shows a series of STM images of the niobia/alumina surface prepared at room temperature at increasing niobia coverage. At 0.1 Å coverage, the particles are randomly dispersed on the surface, i.e. both on and between the line defects (antiphase and reflection domain boundaries, steps) clearly visible in Figure 11a. As previously shown for other metal deposits on the alumina film, the particle spatial distribution basically reflects the degree of metal support interaction (Bäumer and Freund



NIOBIA BASED REAL CATALYSTS AND MODEL SYSTEMS

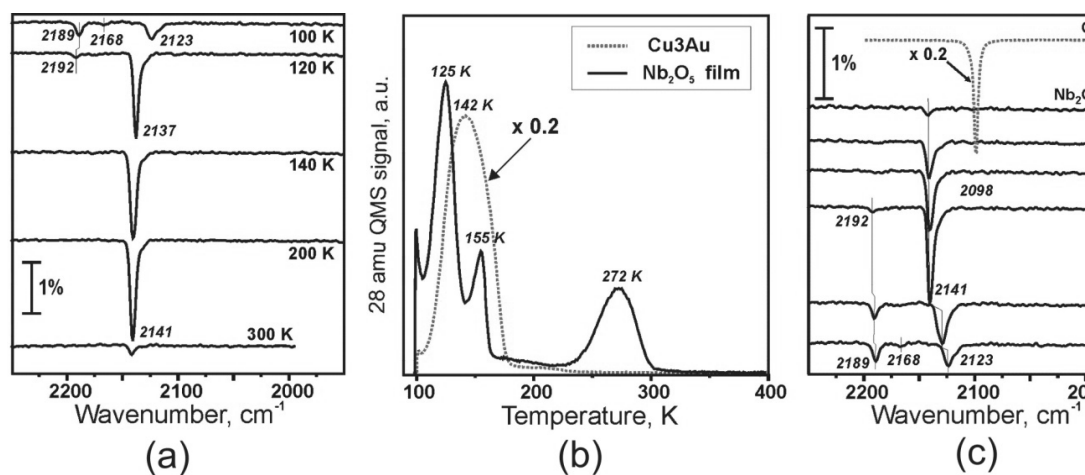
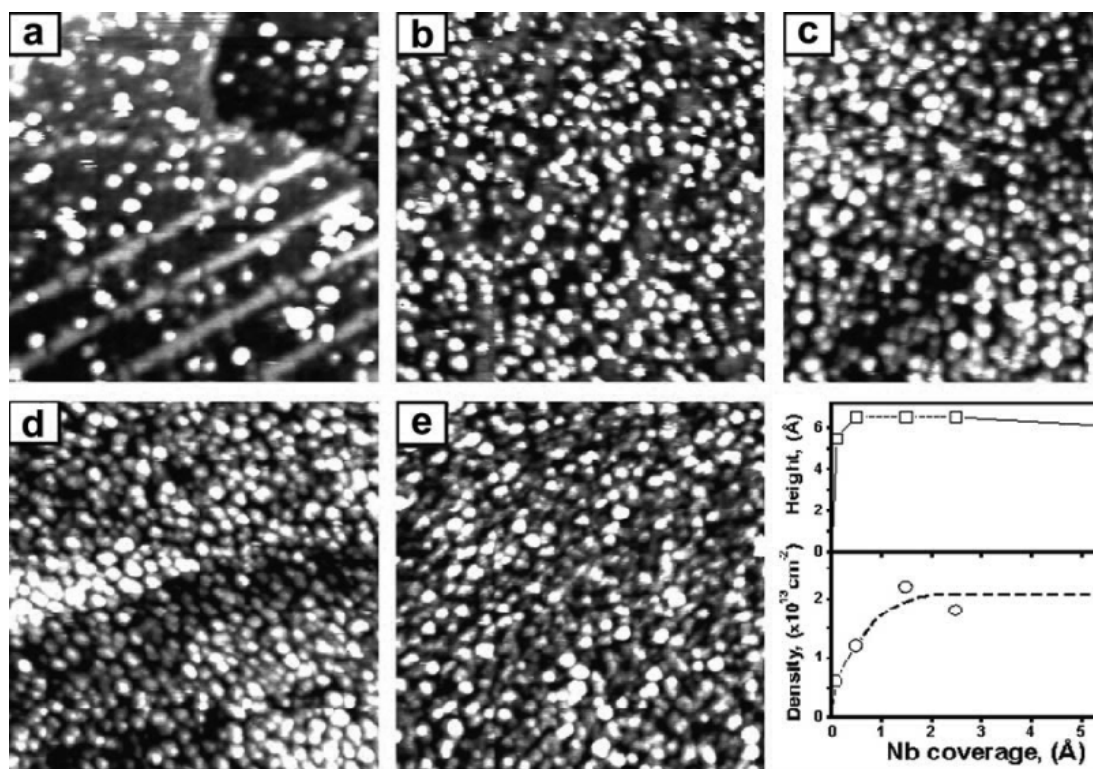
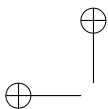


Fig. 10 – (a) Typical TPD spectrum of CO adsorbed on thin niobia films at 100 K. (b) IRAS spectra of CO adsorbed on thin niobia as a function of CO exposure at 100 K. (c) IRAS spectra of CO adsorbed at 100 K and subsequently flashed to the indicated temperature. The TPD and IRAS spectra for a Cu₃Au(100) substrate at saturation CO coverage are also shown in (b) and (c) for comparison (Mendes et al. 2006b).





Nb atoms and the alumina surface. Particle density increases with the coverage up to $\sim 1\text{\AA}$ and then saturates at $\sim 2 \times 10^{13}\text{ cm}^{-2}$, while the average particle height is nearly constant from the onset (see Fig. 11f). Note that, at high coverage, the particle size is difficult to be determined precisely due to the tip deconvolution effect. Obviously, niobia grows in a three-dimensional mode under these conditions. Infrared spectroscopy was used to study the surface structure of the alumina supported niobia particles. The IRAS method allows one to investigate phonon vibrations at oxide surfaces as well as of adsorbates such as CO used here as a probe molecule.

The phonon region of the IRA spectra is shown in Figure 12a. The pristine alumina film exhibits a sharp peak at $\sim 865\text{ cm}^{-1}$ as previously reported (Frank et al. 2001). The alumina phonon attenuates upon niobia deposition and a new band appears as a shoulder at around 900 cm^{-1} , ultimately resulting in a broad signal centered at 885 cm^{-1} for the highest niobia coverage studied. The spectral broadening is consistent with the formation of randomly dispersed small niobia particles as revealed by STM. At the coverage of 1\AA , a band centered at 986 cm^{-1} emerges, which grows in intensity with the coverage. The assignment of these spectral features is facilitated by comparison with the results on a supported vanadia system previously studied in detail (Magg et al. 2003a, 2002, 2004). For convenience, the bottom curve in Figure 12a shows the spectrum obtained for the similarly prepared 3.5\AA vanadia/alumina sample in the same experimental setup. Based on Raman and IR spectroscopy results, the peak at 1045 cm^{-1} has been assigned to the stretching of vanadyl (V=O) groups. Meanwhile, the broad signal at $\sim 950\text{ cm}^{-1}$ is associated with vibrations involving V-O-Al linkage at the vanadia/alumina interface as predicted by theoretical calculations (Magg et al. 2003b, 2002). Therefore, turning back to the niobia/alumina system, the peak at 986 cm^{-1} must be assigned to the niobyl (Nb=O) stretching, and the signal at 890 cm^{-1} must be assigned to Nb-O-Al interface vibrations, which should show lower frequencies as compared to vanadia/alumina, based solely on mass considerations (Nb atom is heavier than V).

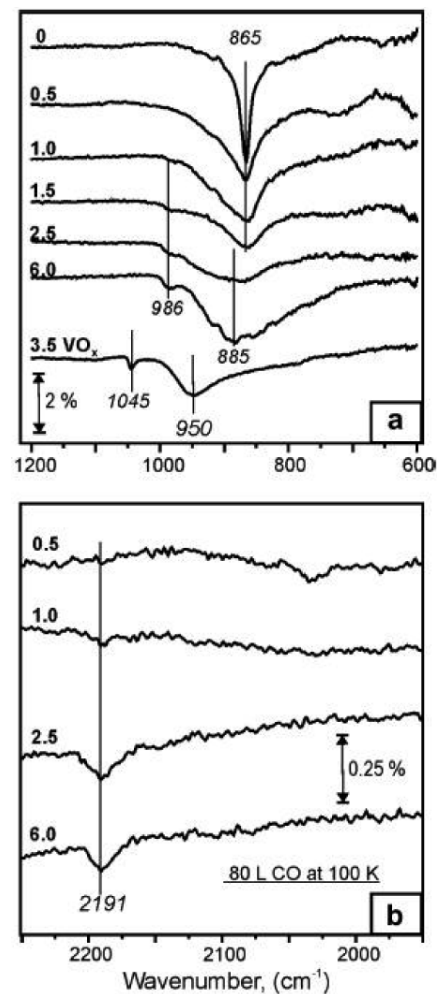
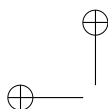


Fig. 12 – (a) The phonon region of IRA-spectra of the niobia/alumina samples as a function of niobia coverage as indicated (in \AA). A spectrum for similarly prepared vanadia/alumina is also shown, for comparison. (b) IRA-spectra of 80 L CO adsorbed at 100 K as a function of niobia coverage. All spectra are offset for clarity (Uhl et al. 2007).

niobia is found to be weak and can be seen only at low temperatures (see Fig. 12b). The strongly blue-shifted frequency of CO as compared to the gas phase ($2191\text{ vs. }2143\text{ cm}^{-1}$) implies that CO is linearly adsorbed on top of Nb^{5+} sites (Beutel et al. 1997, Mendes et al. 2006b). A similar feature at 2190 cm^{-1} was also obtained on the thin niobia films (not shown here), i.e. fully consistent



NIOBIA BASED REAL CATALYSTS AND MODEL SYSTEMS

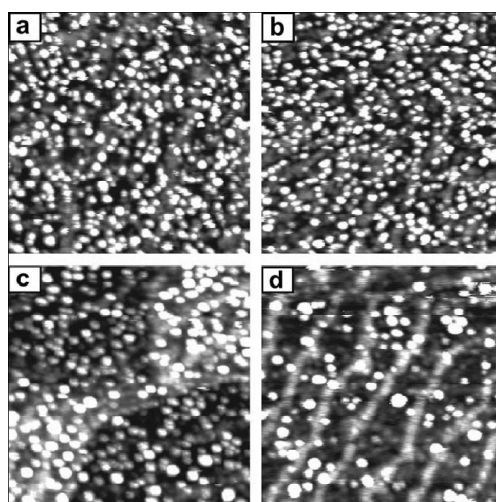


Fig. 13 – STM images (size $60 \times 60 \text{ nm}^2$, $V_S = 3 \text{ V}$, $I = 0.1 \text{ nA}$) of 0.5 Å niobia/alumina samples: (a) as prepared at 300 K; (b)-(d) flashed to 500, 700 and 900 K, respectively. Antiphase domain boundaries are clearly seen in (d) due to migration of the niobia deposits through the line defects and their decoration (Uhl et al. 2007).

particles terminated by the Nb=O groups and also Nb^{5+} sites. Thermal stability of the supported niobia particles was further examined by STM and IRAS.

Figure 13 shows STM images of the 0.5 Å niobia/alumina sample after a thermal flash to elevated temperatures (500–900 K) in UHV. Annealing to 700 K basically decreases the particle density partially due to sintering of the particles (some particles gain in size) and also due to niobia migration into the film, which is more clearly observed after annealing to 900 K. As previously shown for other metal particles (Heemeier et al. 2003), the interdiffusion probably goes through the line defects of the alumina film, thus resulting in their decoration (see Fig. 13d).

The 2.5 Å niobia/alumina sample, shown in Figure 14a, was first flashed in UHV to 700 K, then oxidized in 10^{-7} mbar O_2 at 400 K and finally at 900 K. One can see that, in contrast to annealing in UHV, ambient oxygen precludes the migration of the niobia particles, and only partial sintering occurs at 900 K.

Figure 15 shows the results of a complementary

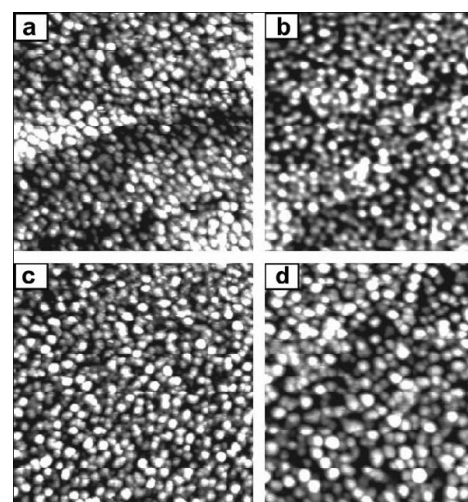


Fig. 14 – STM images (size $60 \times 60 \text{ nm}^2$, $V_S = 3 \text{ V}$, $I = 0.1 \text{ nA}$) of 2.5 Å niobia sample: (a) as prepared at 300 K; (b) flashed to UHV; (c, d) flashed to 400 K (c) and then to 900 K (d) in 10^{-7} mbar O_2 . Note smaller morphological changes for the oxidized sample compared to the UHV annealed samples (see Fig. 7) (Uhl et al. 2007).

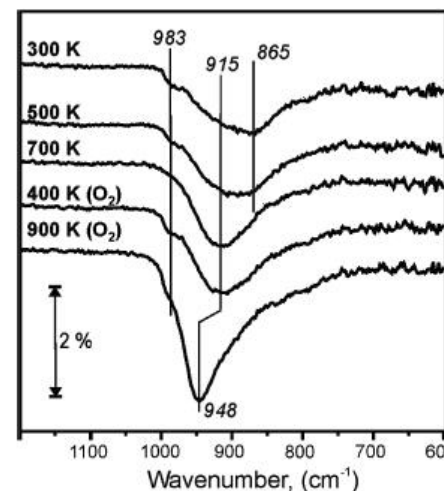
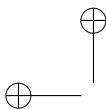


Fig. 15 – IRAS-spectra of 2.5 Å niobia sample annealed to the indicated temperature and subsequently oxidized in $10^{-7} \text{ mbar of O}_2$ and then at 900 K. The Nb=O band at 983 cm^{-1} disappeared and is recovered upon oxidation treatment. All measurements were performed at room temperature. The spectra are offset for clarity (Uhl et al. 2007).

band centered at $\sim 900 \text{ cm}^{-1}$ and assigned to



can be explained by the onset of niobia migration as revealed by STM and discussed above. Mild oxidation at 400 K recovers the niobyl species without affecting the interface region. However, further oxidation at 900 K shifts the interface phonon from 915 cm^{-1} to 948 cm^{-1} (partially overlapping with the Nb=O band). This shift can be related to the structural transformations of the niobia/alumina interface since the STM results showed that overall particle morphology is not affected much by oxidation at 900 K. Note also that this finding indirectly supports our previous assignment of the $\sim 900\text{ cm}^{-1}$ band to niobia/alumina interface phonon. The effect of ambient oxygen on the thermal stability of the niobia particles can be rationalized in terms of oxygen preventing the reduction of the niobia surface and hence migration of the Nb atoms into the film. In addition, previous studies on the oxygen interaction with alumina supported particles showed that the metal particles may promote thickening of the alumina film via oxygen dissociation and subsequent diffusion of atomic oxygen to the alumina/NiAl interface (Bäumer et al. 1999, Shaikhutdinov et al. 2002). This in turn may also alter the interaction of the niobia particles and the alumina film.

Elemental metal particles have been studied extensively on a number of bulk single crystal and thin film oxide supports (Campbell 1997, Henry 1998, Freund 1997, Freund and Pacchioni 2008, Goodman 1995). For the latter case, which is the subject of the current discussion, we refer to a number of reviews. Co and/or Pd particles have been studied on aluminum (Bäumer and Freund 1999) and on niobia (Bäumer and Freund 1999, Höbel et al. 2006), as well as on alumina supported niobia (Uhl et al. 2007). Co-Pd alloy particles so far exclusively on the alumina support (Heemeier et al. 2002).

Co binds strongly to alumina while the metal remains in its metallic state. Figure 16a shows an STM image of 2Å of deposited Co at room temperature. There is a strong propensity to form lower coordinated metal atoms on the nanoparticle at low temperature, as may be identified by IRAS studies (Risse et al. 2003). Co particles lose those low coordinated sites and sinter

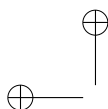
(Carlsson et al. 2003c). The latter technique delivers detailed insight not only into sintering but also into the rearrangement at the surfaces of the particles, including the metal oxide interface. This is due to energetically separated surface resonances in FMR spectroscopy, which allows for separate investigation by gas adsorption at the metal vacuum and by temperature changes on the metal oxide interface (Risse et al. 2004). Pd binds less strongly to the alumina surface and forms relatively large metallic particles at room temperature. These particles are located at line defects (i.e. antiphase domains boundaries) of the film and form small, almost ideal single crystals of truncated cuboctahedral morphology. Figure 16b shows an STM image of a Pd nanoparticle distribution along with a high resolution image revealing the surface atoms in the well ordered facets. Using CO as a probe molecule, the surface sites have been characterized in detail.

Nanometer-sized Co-Pd alloy nanoparticles were generated by sequentially depositing the two constituents onto alumina.

Inspired by earlier work by Henry and co-workers (Gimenez et al. 1998, Giorgio et al. 1999), different structures and compositions of the particles were obtained in a controllable way by taking advantage of the different nucleation and growth properties of the two metals.

Let us now assume that Pd is deposited on a surface already covered by Co particles. Owing to the higher mobility of Pd on the surface, it will be trapped at Co particles before reaching the line defects. The STM image presented in Figure 17 essentially corroborates this expectation. The arrangement of particles found for this sequence strongly resembles that for pure Co, thus suggesting particles with a Co core and a Pd shell. If, on the other hand, Pd is deposited first, the less mobile Co atoms should partly cover the Pd crystallites and partly nucleate between them. The STM image indeed shows triangular and hexagonal crystallites as well as the large number of new small clusters between them.

To verify the surface composition of the alloy particles, we performed both temperature programmed des-



NIOBIA BASED REAL CATALYSTS AND MODEL SYSTEMS

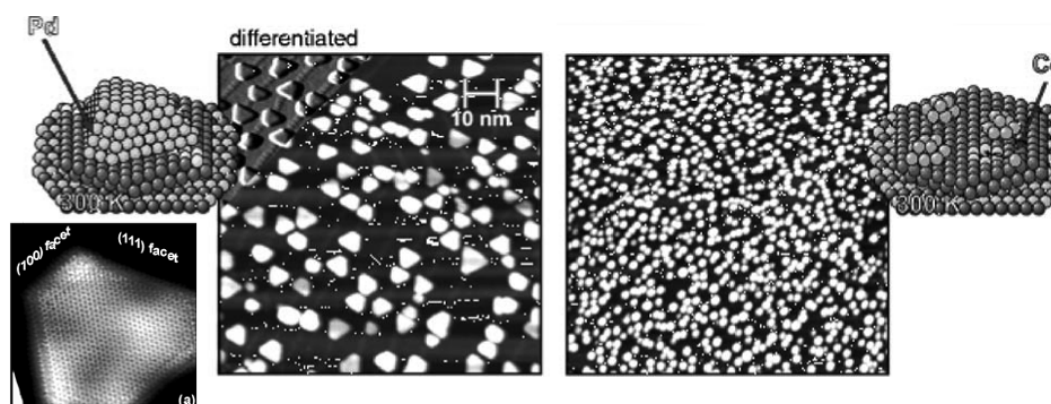


Fig. 16 – Sequential deposition of Co and Pd and *vice-versa* onto a thin alumina film at 300 K. The ball models schematically show the structure of the systems investigated: gray: NiAl substrate; blue: Al_2O_3 film; light blue: defects of the alumina film; yellow: Pd atoms; orange: Co atoms (Hansen et al. 1999, Heemeier et al. 2002).

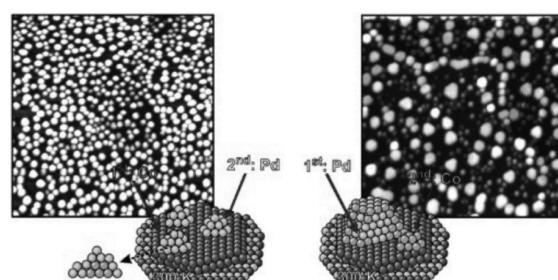


Fig. 17 – STM images ($100 \text{ nm} \times 100 \text{ nm}$) taken after depositing 2 \AA Pd and 2 \AA Co alone. The ball models schematically show the structure of the systems investigated: gray: NiAl substrate; blue: Al_2O_3 film; light blue: defects of the alumina film; yellow: Pd atoms; orange: Co atoms (Heemeier et al. 2002).

the two metals. Without repeating the discussion given in the original papers, we can infer the growth mode and the surface composition qualitatively from the schematic representation in Figure 18.

This information is not only based on TDS and IRAS data but also on STM and XPS data collected by Carlsson et al. (2003a, b, c). Pd deposition onto Co results in a core shell situation, while the reverse deposition sequence results in a more homogeneous alloy particle with some Co within the surface layer.

The interaction of Co with niobia is completely different. Even though we have to stress that so far, only

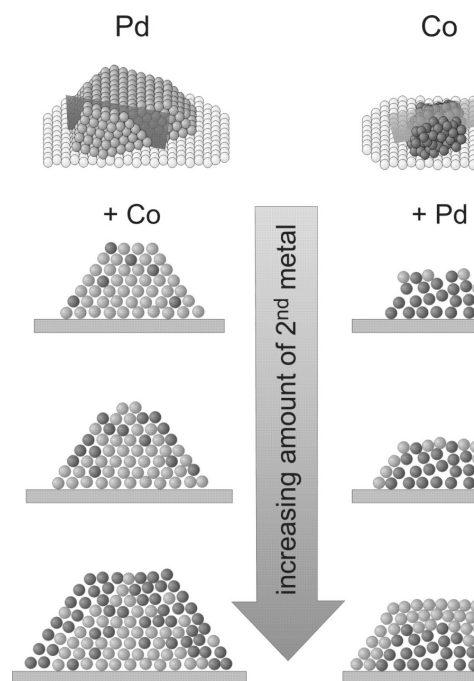


Fig. 18 – Schematic representation of the growth mode as a function of the amount of the second metal, deduced from IRAS, TPD, XPS, and STM data (Carlsson et al. 2003c).

Figure 19 shows STM images of Co deposited on the niobia films at two Co coverages, 1 \AA (a and b) and 2 \AA (c and d), respectively. It is clear

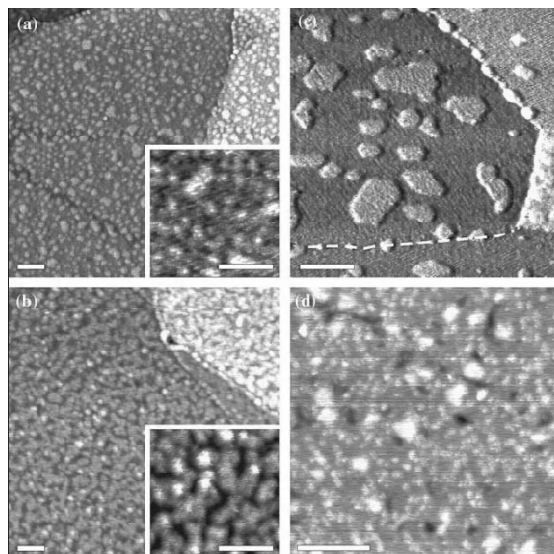
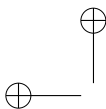
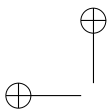


Fig. 19 – STM images of Co deposited at 300 K on thin niobia films. The Co coverage is 0.5 Å (a and c) and 2 Å (b and d). Images (c) and (d) are taken after heating the same samples to 500 K. The scale bar corresponds to 20 nm. Tunneling parameters are: (a) bias 1.2 V, current 1 nA; (b) 0.75 V, 0.7 nA; (c) 1.25 V, 1.3 nA; (d) 0.75 V, 1 nA. Image (c) is presented in differentiated contrast, where the domain boundary is marked by the dash line (Mendes et al. 2006b).

implies that Co essentially wets the surface and forms two-dimensional, monolayer islands at 300 K. Since the formation of these islands can be kinetically limited, we have examined the surface after annealing to 500 K, which resulted in large well-shaped monolayer islands at low Co coverage (Fig. 19c). At high Co coverage, the ill-defined and relatively rough surface, with a corrugation amplitude of ca. 1 Å, is observed in Fig. 19d. Note that this morphology is very different from Co deposited on thin alumina films, in which three-dimensional particles up to 2 nm in height are formed under these conditions (Hill et al. 1998).

The electronic structure of the Co species on the niobia films was studied by Photoelectron Spectroscopy (PES) using synchrotron radiation. Figure 20 shows PES spectra before and after Co deposition at 300 K. The clean film is characterized by the binding energies (BE) of the Nb 3d_{5/2} level at 206.4 eV and of the O 1s level at

screening effect of the metal substrate underneath oxide films. For Co deposited at 300 K the PE-spectra show two species characterized by BE of Co 2p_{3/2} at 778 and 781 eV. These values are typical for metallic (Co⁰) and oxidized (Co^{δ+}, like in Co₃O₄ or CoO) states, respectively [XPS and AES Database, Thermo Electr. Corp. <http://www.lasurface.com/database/element.php>]. The Co^{δ+}:Co⁰ integral ratio increases from 0.1 to 0.3 when the spectrum is measured at grazing incidence. This indicates that Co^{δ+} species are on the surface, while metallic Co is mostly located in the subsurface region. In principle, this could be explained by the formation of the Co particles with oxidized Co^{δ+} species on the surface modified by Nb⁵⁺ as revealed by CO IRAS. However, the STM images presented in Figure 19 did not show the three-dimensional particles but single layer islands, which are typical for the morphology of metal-on-metal systems. Therefore, it seems likely that Co migrates through the film and forms a metallic layer directly bonded to the Cu₃Au(100) substrate. In this model, the oxidized Co^{δ+} species are formed on or incorporated into the niobia film, thus resulting in a partial reduction of the niobium cations. The formation of two Nb species is clearly seen in the Nb3d spectrum of the Co/niobia sample, which splits into two components, centered at 207.1 and 206.2 eV for the Nb 3d_{5/2} level, (after deconvolution not shown here). The ratio between these two signals does not depend on the detection angle as shown in Figure 20, which suggests that all Nb species lie in a single layer as in the original film (see Fig. 8d). The component at 207.1 eV deserves a comment since the binding energy is higher than in the original niobia film, where Nb is already in its highest oxidation state, 5+. We tentatively attribute this effect to the presence of cobalt ions and reduced niobia ions in the film, which probably pin the Fermi level at a different position. Although the precise structure of this mixed Co-Nb oxide phase needs further studies, the PES results clearly show that Co deposited on the niobia film can be readily oxidized at room temperature, which is in contrast to Co deposits on the alumina films (Carlsson et al. 2003a, Hill et al. 1998).



NIOBIA BASED REAL CATALYSTS AND MODEL SYSTEMS

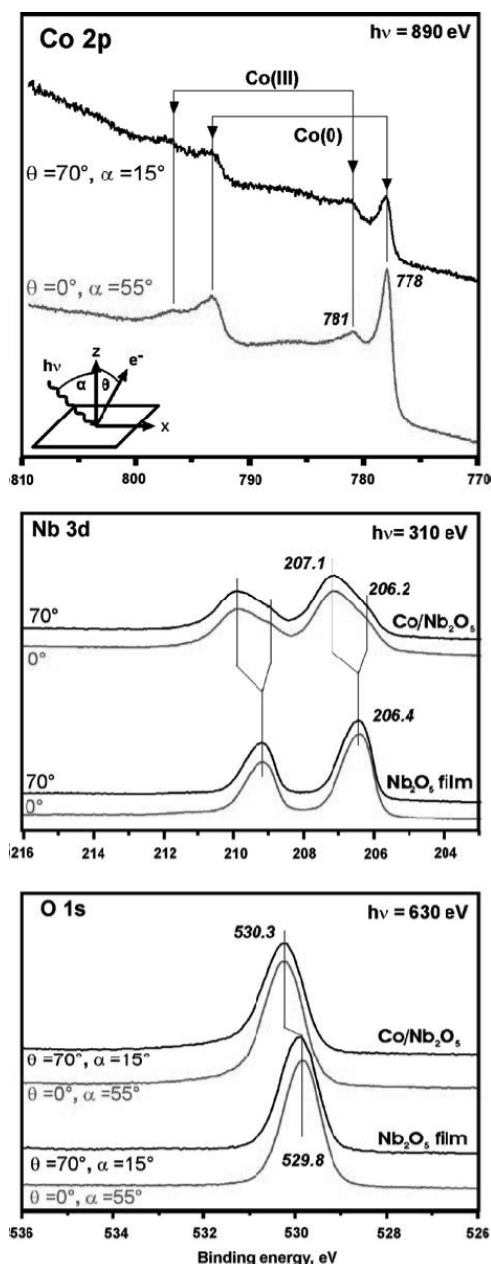
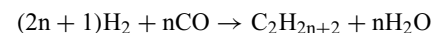


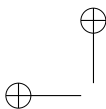
Fig. 20 – Co2p, Nb3d and O1s regions of photoelectron spectra measured at two different geometries as depicted in the inset. The spectra for Nb and O core levels are shown before and after 2 Å of Co have been deposited at 300 K (Mendes et al. 2006b).

and from UHV to 100 mbar. Annealing Pd-Cu₃Au(100) higher than 300 K lead to irreversible structural changes, indicated by a ~50% loss of adsorption capacity and pronounced changes in adsorption states. Changes in the vibrational frequencies and phase in CO-SFG spectra suggest alteration of the electronic structure of the model catalyst by support interaction, i.e. formation of “mixed Pd compounds”, while simple structural changes or sintering of the Pd particles can be excluded. Furthermore, the new surface composition is different from pure Pd, i.e. migration of Nb₂O₅ over Pd particles cannot explain the current findings. These effects were observed both under UHV and ambient pressure and may contribute to the catalytic properties of Nb₂O₅ supported metal nanoparticles.

After having studied the morphological, structural, electronic and adsorption properties of the materials in question, it is very important to move on to their reactivity which in turn allows us the most detailed comparison to the real catalyst. So far, reactivity studies on model systems have only been performed on Co and Co alloy particles on alumina (Carlsson et al. 2000). Those reactivity studies are governed by the fact that the target reactions are of Fischer-Tropsch type,



Co is a well known Fischer-Tropsch catalyst but it, however, deactivates upon oxidation. It has been proposed that the addition of Pd promotes the reduction of Co oxide by activating hydrogen. In order to shed light on this question we have studied adsorption and reactivity of molecules relevant for a Fischer-Tropsch synthesis, i.e. oxygen, hydrogen, carbonmonoxide, and water. The point to note is the influence of oxygen on the reduction of oxidation of the particles and the concomitant influence on the reaction behavior. A rather detailed study on oxygen adsorption and sample annealing employing a combination of XPS, IRAS, TPD, and FMR showed that oxidation involves diffusion of oxygen into the support and, after stabilization, a combination of surface and subsurface oxygen is formed, leaving the



Two limiting cases have been studied: i) incomplete Pd shell, ii) thick Pd shell. While the incomplete shell leads to facilitated oxidation, the full Pd shell suppresses it entirely.

Hydrogen and CO adsorption is facile on the non-oxidized particles, but is severely inhibited on the oxidized bimetallic and pure Co particles; Pd particles become covered with a chemisorbed oxygen overlayer which still allows a small amount of H₂ adsorption. This suggests that oxidized Co or Co-Pd particles should be less active than unoxidized ones in the Fischer-Tropsch conversion of CO+H₂ to higher hydrocarbons because CO and H₂ cannot adsorb. The interaction of ethylene with the bimetallic Co-Pd particles is similar to the interaction of ethylene with Pd or Co particles, in which it is π -bonded below 230 K and di- σ bonded from \sim 230 to 270 K. At 270 K it begins to desorb or decompose to form ethylidyne, liberating hydrogen. In contrast, on the oxidized Co-containing particles, ethylene is only able to adsorb in the π -bonded state and to form the di- σ bonded state. The formation of ethylidyne, is inhibited as well. To slightly different degrees, the bimetallic or monometallic particles are active for ethylene hydrogenation; the oxidized particles are essentially non-active for ethylene hydrogenation. These reactive studies indicate that the reduction of CoO to metal could be of prime importance for the Fischer-Tropsch reaction.

SYNOPSIS

What have we learned?

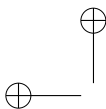
- It is possible to prepare and characterize different model support materials such as alumina, niobia and alumina supported niobia and characterize them at the atomic level, thus forming the basis for a comparison with “real” support materials. Model studies have provided detailed information of the support surfaces which are difficult to deduce for the real catalyst support. Clearly, the full complexity of the real material has not been modeled yet, and further studies are needed. However, the strategy to build up models starting with the simple systems and procedures bottom up clearly is the strategy of

model systems. In particular, alloy formation may directly be followed providing useful information for studies on real catalysts in which such a proof is difficult to deliver.

- It is possible to follow the strong metal support interaction suggested by studies on real catalysts on the model systems for niobia supports and not for alumina supports. The suggested formation of Co²⁺ penetration into the niobia lattice can be fully supported.
- Due to the well defined morphology of model systems, it is possible to get deduce the distribution of the oxide and the metal in the particles. The same is true for the distribution of the metal composition upon alloy formation.
- It is shown for both real catalysts and model systems that Co oxidation plays a key role in controlling the reactivity of the system and that the addition of Pd is a determining factor with respect to the interaction with hydrogen and oxidation.
- It is demonstrated that the interaction with unsaturated hydrocarbons depends strongly on the state of oxidation of the particles.

So we have learned a lot but certainly not enough to say we have a full understanding of the phenomena in this particular case. Work has to be done on both sides: Models have to be made more stable to endure higher temperatures for treatment. Also, more frequently techniques have to be applied, such as sum frequency generation that allows us to go to ambient conditions. More sophisticated techniques have to be applied to real catalysts, such as aberration corrected transmission electron microscopy, which would allow us to look at those systems closer to the atomic level and compare them with scanning probe data gained on the models.

We believe that such a joint effect between groups working on catalysis with an applied touch and groups trying to improve a more basic understanding of the phenomena is very beneficial for both sides and the scientific community as a whole because, by working collaboratively, one develops not only scientific understanding but also trust in the work of others. The latter is crucial



NIOBIA BASED REAL CATALYSTS AND MODEL SYSTEMS

ACKNOWLEDGMENTS

The second author thanks the Deutsche Forschungsgemeinschaft through SFB 546 and the Fonds der Chemischen Industrie for financial support. The first author is grateful to the Humboldt Foundation for a Humboldt Award, as well as Coordenação de Aperfeiçoamento de Pessoal de Nível Superior/Deutsche Forschungsgemeinschaft (CAPES/DFG) for interchange Brazil/Germany program and Conselho Nacional de Desenvolvimento Científico e Tecnológico (CNPq) for financial support and Coordenação de Pós-Graduação e Pesquisa em Engenharia/ Programa de Engenharia Química/ Núcleo de Catálise/ Universidade Federal do Rio de Janeiro (COPPE/PEQ/Nucat/UFRJ) for supporting this work.

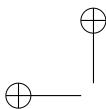
RESUMO

As ciências da catálise e da superfície têm desenvolvido independentemente temas básicos para o entendimento de processos catalíticos. Pode-se até questionar se há ainda algo fundamental para ser descoberto através da interface entre catálise e ciência da superfície?

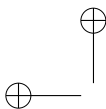
Catalisadores mono e bimetalícos de Co/Nb₂O₅ e Pd-Co/Nb₂O₅ apresentaram resultados interessantes de seletividade na síntese de Fischer-Tropsch (Noronha et al. 1996, Rosenir et al. 1993). A presença de metal nobre aumentou a seletividade de C₅⁺ e diminuiu a formação de metano dependendo da temperatura de redução. Catalisadores modelo de Co-Pd suportados em nióbia e alumina foram preparados e caracterizados a nível atômico, servindo de base para comparação do catalisador “real”. Foram estudados o crescimento de partículas, bem como a morfologia e a estrutura de partículas de ambos, metal puro e ligas. É possível suportar as propostas que sugerem uma forte interação metal suporte em catalisadores reais através das pesquisas em sistemas modelos para nióbia quando comparadas com suportes de alumina onde estes efeitos não aparecem. A formação de Co²⁺ penetrando na rede da nióbia, sugerida para catalisadores em forma de pó, foi totalmente confirmada pelos estudos em catalisadores modelo. Mostrou-se ainda que para ambos os sistemas reais e modelos, que o estado oxidado do Co tem papel fundamental na reatividade das reações de Fischer-Tropsch e que a adição de Pd é um fator determinante para a estabilidade do catalisador. Demonstrou-se que a interação com hidrocarbonetos insatura-

REFERENCES

- AHON VR, LAGE PLC, DE SOUZA CDD, M...
FMT AND SCHMAL M. 2006. J Nat Gas Chem 1...
312.
- ANDERSON RB. 1984. The Fischer-Tropsch Synthe...
lando: Academic Press Inc.
- ARNOLDY P AND MOULIJN JA. 1985. Temperat...
grammed reduction of CoO/Al₂O₃ catalysts. J C...
38–54.
- BÄUMER M AND FREUND H-J. 1999. Metal Dep...
Well-ordered Oxide Films. Progr Surf. Sci 61: 12...
- BÄUMER M, BIENER J AND MADIX RJ. 1999. ...
electronic properties and reactivity of vanadium d...
onto a thin alumina film. Surf Sci 432: 189–198.
- BEUTEL T, SIBOROV V, TESCHE B AND KNÖZIN...
1997. Strong Metal-Promoter Oxide Interactions...
by Calcination in V, Nb, and Ta Oxide Promoted F...
Catalysts. J Catal 167: 379–390.
- BLYHOLDER G. 1964. Molecular Orbital View of C...
orbed Carbon Monoxide. J Phys Chem 68: 2772–
- CAMPBELL CT. 1997. Ultrathin metal films and part...
oxide surfaces: structural, electronic and chemi...
properties. Surf Sci Rep 27: 1–111.
- CARLSSON AF, BÄUMER M, RISSE T AND FREU...
2003a. Surface structure of Co-Pd bimetallic p...
supported on Al₂O₃ thin films studied using infr...
flexion absorption spectroscopy of CO. J Chem Pl...
10885–10894.
- CARLSSON AF, NASCHITZKI M, BÄUMER M AND F...
HJ. 2003b. Adsorption and reaction on pristine e...
dized Co-Pd bimetallic particles supported on Al₂...
films. Surf Sci 545: 143–153.
- CARLSSON AF, NASCHITZKI M, BÄUMER M AN...
UND HJ. 2003c. The structure and reactivity of...
supported Cobalt-Palladium Particles: a CO-TPI...
and XPS study. J Phys Chem. B. 107: 778–785.
- CASTNER DG AND SANTILLI DS. 1984. In: WHY...
DALLA BETA RA, DEROUANE EG, BAKER RT...
Catalytic Materials: Relationship between Struct...
Reactivity, ACS Symposium Series, p. 39.
- CATALANO JG, PARK C, FENTER PA AND ZHANG...
Simultaneous Inner- and Outer Sphere Arsenate...
tion on Corundum and Hematite Method: X-ray so...
(XPS). Geochim Cosmochim Acta 72: 1986–2000.

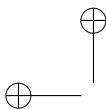


- DATTA AK, HA J-W AND REGALBUTO JR. 1992. The controlled dispersion of silica supported MoO₃: The role of ammonia. *J Catal* 133: 55–82.
- DAVYDOV AA. 1984. *Infrared Spectroscopy Of Adsorbed Species on the Surface of Transition Metal Oxides*. John Wiley & Sons, 243 p.
- DIEBOLD U. 2003. The surface science of titanium dioxide. *Surf Sci Rep* 48: 53–229.
- DRY ME. 1981. Springer Verlag, Berlin, p. 159.
- ERTL G. 2008. Reactions at Surfaces: From Atoms to Complexity (Nobel Lecture). *Angew Chem Int Ed.* 47: 3524–3535.
- FRANK M, WOLTER K, MAGG N, HEEMEIER M, KUHNEMUTH R, BÄUMER M AND FREUND H-J. 2001. Phonons of clean and metal-modified oxide films: an infrared and HREELS study. *Surf Sci* 492: 270–284.
- FREUND H-J. 1997. Adsorption of gases on complex solid surfaces [Review]. *Angew Chem Int Ed.* 36: 452–475.
- FREUND H AND GOODMAN DW. 2007. Ultrathin Oxide Films. In: ERTL G, KNÖZINGER H, SCHÜTH F, WEITKAMP J (Eds), *Handbook of Heterogeneous Catalysis*, 2nd ed., Wiley-VCH Verlagsgesellschaft mbH: Weinheim.
- FREUND H-J AND PACCHIONI G. 2008. Oxide ultra-thin films on metals: new materials for the design of supported metal catalysts. *Chem Soc Rev* 37: 2224–2242.
- FREUND H-J, KUHLENBECK H AND STAEMMLER V. 1996. Oxide Surfaces [Review]. *Rep Progr Phys* 59: 283–347.
- FREUND H-J, LIBUDA J, BÄUMER M, RISSE T AND CARLSSON AF. 2003. Cluster, Facets and Edges: Site Dependent Selective Chemistry on Model Catalysts. *Chem Rec* 3: 181–200.
- FU L AND BARTHOLOMEW CH. 1985. Structure sensitivity and its effects on product distribution in CO hydrogenation on cobalt/alumina. *J Catal* 92: 376–387.
- GIMENEZ F, CHAPON C AND HENRY CR. 1998. *New J Chem* 22: 1289.
- GIORGIO S, CHAPON C AND HENRY CR. 1999. In: BRAUNSTEIN P, ORO LA, RAITHBY PR (Eds), *Metal Clusters in Chemistry*, Wiley-VCH: Weinheim, p. 1194.
- GOODMAN DW. 1995. Model catalysts – from extended single crystals to supported particles. *Surf Rev Lett* 2: 9–24.
- GRAHAM GW. 1987. Carbon monoxide chemisorption on Cu₃Au(100) and related surfaces. *Surf Sci* 187: 490–498.
- GUCZI L, HOFFER T, ZSOLDOS Z, ZYADE S, MAIRE G AND GARIN F. 1991. Structure and catalytic activity of
- HANSEN KH, WORREN T, STEMPER S, LAEGSGAARD E, BÄUMER M, FREUND HJ, BESENBACHER F AND STENSGAARD I. 1999. Palladium Nanocrystals on Al₂O₃: Structure and Adhesion Energy. *Phys Rev Lett* 83: 4120.
- HEEMEIER M, CARLSSON A, NASCHITZKI M, SCHMAL M, BÄUMER M AND FREUND HJ. 2002. Preparation and characterization of a model bimetallic catalyst: Co-Pd nanoparticles supported on Al₂O₃. *Angew Chem Int Ed.* 41: 4073–4074.
- HEEMEIER M, STEMPER S, SHAIKHUTDINOV SK, LIBUDA J, BÄUMER M, OLDMAN RJ, JACKSON SD AND FREUND H-J. 2003. On the thermal stability of metal particles supported on a thin alumina film. *Surf Sci* 523: 103–110.
- HENRY CR. 1998. Surface studies of supported model catalysts. *Surf Sci Rep* 31: 231–326.
- HILL T, MOZAFFARI-AFSHAR M, SCHMIDT J, RISSE T, STEMPER S, HEEMEIER M AND FREUND H-J. 1998. Influence of CO Adsorption on the Magnetism of Small CO Particles Deposited on Al₂O₃. *Chem Phys Lett* 292: 524–530.
- HILL T, RISSE T AND FREUND H-J. 2005. Reorganization of small Co particles on Al₂O₃ surfaces monitored by ferromagnetic resonance. *J Chem Phys* 122: 164704- 1–9.
- HO SW, HOUALLA M AND HERCULES DM. 1990. Effect of particle size on carbon monoxide hydrogenation activity of silica supported cobalt catalysts. *J Phys Chem* 94: 6396–6399.
- HO SW, CRUZ JM, HOUALLA M AND HERCULES DM. 1992. The structure and activity of titania supported cobalt catalysts. *J Catal* 135: 173–185.
- HÖBEL F, BANDARA A, RUPPRECHTER G AND FREUND H-J. 2006. Deactivation of Pd particles supported on Nb₂O₅/Cu₃Au(100): SFG and TPD studies from UHV to 100 mbar. *Surf Sci* 600: 963–970.
- IDRISS H, DIAGNE C, HINDERMANN JP, KINNEIMANN A AND BARTEAU MA. 1992. In: GUCZI L, SOLYMOSI F, TETENYI P (Eds), *Proceedings of the 10th International Congress on Catalysis*, Elsevier: Budapest, Vol. Part C, p. 2119.
- JAEGER RM, KUHLENBECK H, FREUND H-J, WUTTIG M, HOFFMANN W, FRANCHY R AND IBACH H. 1991. Formation of a well-ordered aluminium oxide overlayer by oxidation of NiAl(110). *Surf Sci* 259: 235.
- JUSZCZYK W, KARPINSKI Z, LOMOT D, PIELASZEK J, BAL Z AND STAKHEEV AY. 1993. The Structure and



NIOBIA BASED REAL CATALYSTS AND MODEL SYSTEMS

- KAPOOR MP, LAPIDUS AL AND KRYLOVA AY. 1992. In: GUCZI L, SOLYMOSI F, TETENYI P (Eds), *Proceedings of the 10th International Congress on Catalysis*, Budapest, Elsevier: Budapest, p. 2741.
- KIM JG, SHYU JZ AND REGALBUTO JR. 1993. The Effect of Calcination on H₂ Spillover in Pt/MoO₃: I. Characterization and Kinetics. *J Catal* 139: 153–174.
- KRESSE G, SCHMID M, NAPETSCHNIG E, SHISHKIN M, KÖHLER L AND VARGA P. 2005. Structure of the Ultrathin Aluminum Oxide Film on NiAl(110) *Science* 308: 1440–1442.
- KULAWIK M, NILIUS N AND FREUND HJ. 2006. Influence of the Metal Substrate on the Adsorption Properties of Thin Oxide Layers: Au Atoms on a Thin Alumina Film on NiAl(110). *Phys Rev Lett* 96: 036103- 1–4.
- LAPIDUS A, KRYLOVA A, KAZANSKII V, BOROVKOV V, ZAITSEV A, RATHOUSKY J, ZUKAL A AND JANCÁLKOVÁ M. 1991. Hydrocarbon synthesis from carbon monoxide and hydrogen on impregnated cobalt catalysts Part I. Physico-chemical properties of 10% cobalt/alumina and 10% cobalt/silica. *Appl Catal* 73: 65–81.
- LEE J-H, LEE D-K AND IHM S-K. 1988. Independent effect of particle size and reduction extent on CO hydrogenation over alumina-supported cobalt catalyst. *J Catal* 113: 544–548.
- LIBUDA J, WINKELMANN F, BÄUMER M, FREUND H-J, BERTRAMS T, NEDDERMEYER H AND MÜLLER K. 1994. Structure and defects of an ordered alumina film on NiAl(110). *Surf Sci* 318: 61–73.
- MAGG N, GIORGI JB, SCHROEDER T, BÄUMER M AND FREUND HJ. 2002. Model Catalyst Studies on Vanadia Particles Deposited onto a Thin-Film Alumina Support. 1. Structural Characterization. *J Phys Chem B* 106: 8756–8761.
- MAGG N, GIORGI JB, HAMMOUDEH A, SCHROEDER T, BÄUMER M AND FREUND HJ. 2003a. Model Catalyst Studies on Vanadia Particles Deposited onto a Thin-Film Alumina Support. 2. Interaction with Carbon Monoxide. *J Phys Chem B* 107: 9003–9010.
- MAGG N, GIORGI JB, SCHROEDER T, BÄUMER M AND FREUND H-J. 2003b. Model Catalyst Studies on Vanadia. *J Phys Chem B* 106: 8756–8761.
- MAGG N ET AL. 2004. Vibrational Spectra of Alumina- and Silica-supported Vanadia Revisited: An Experimental and Theoretical Model Catalyst Study. *J Catal* 226: 88–100.
- and Oxidation (TPO) of Co/TiO₂ and Co-Rh/TiO₂ 97: 200–209.
- MENDES FMT, PEREZ CAC, NORONHA FB, SOUZA CESAR DV, FREUND HJ AND SCHMAL M. 2000. Fischer-Tropsch Synthesis on Anchored Co/Nb₂O₅ Catalysts: The Nature of the Surface and the Ethylene Chain Growth. *J Phys Chem B* 110: 9155–9163.
- MENDES FMT, UHL A, STARR DE, GUIMOND S, SCHMAL M, KUHLENBECK H, SHAIKHUTDINOV S AND FREUND HJ. 2006b. Strong metal support interaction on Co/niobia model catalysts *Catal Lett* 111: 35–41.
- MIDDEKE J, BLUM R-P, HAFEMEISTER M AND NIELSEN J. 2005. Controlled preparation of well-ordered transition metal oxide layers on a metallic surface. *Surf Sci* 579: 219–228.
- MORRIS D, DOU Y, REBANE J, MITCHELL CEJ, FLETCHER RG, LAW DSL, VITTADINI A AND CASARIN M. 2005. Photoemission and STM study of the electronic structure of Nb-doped TiO₂. *Phys Rev B* 61: 13445–13451.
- NIEMANTSVERDIET JW, LOIUWERS PA, GROUDEMANS KRAAN AMVD, KAMPERS FWH AND KONINKHOF GER DC. 1988. In: *PROCEEDINGS OF THE 9TH INTERNATIONAL CONGRESS ON CATALYSIS*, Calgary, Canada: Inst Canada: Ottawa, Vol. 2, p. 674.
- NORONHA FB, FRYDMAN A, ARANDA DAG, PEREIRA SOARES RR, MORAWEK B, CASTNER D, CAMARGO CT, FRET Y R AND SCHMAL M. 1996. The promoting effect of noble metal addition on niobia-supported catalysts. *Catal Today* 28: 147–157.
- NORONHA FB, PEREZ CAC, SCHMAL M AND FREUND HJ. 1999. Determination of cobalt species in niobia supported catalysts. *Phys Chem Chem Phys* 1: 2861–2867.
- NORONHA FB, ARANDA DAG, ORDINE AP AND SCHMAL M. 2000a. The promoting effect of Nb₂O₅ addition on Pd/Al₂O₃ catalysts on propane oxidation. *Catal Today* 57: 275–282.
- NORONHA FB, SCHMAL M, MORAWEK B, DELGADO P, BRUN M, VILLAIN F AND FRET Y R. 2000b. Characterization of niobia-supported palladium-cobalt catalysts. *J Phys Chem B* 104: 5478–5485.
- NOWAK I AND ZIOLEK M. 1999. Niobium Compounds: Preparation, Characterization, and Application in Heterogeneous Catalysis. *Chem Rev* 99: 3603–3624.
- NOWITZKI T, CARLSSON AF, MARTYANOV O, NIELSEN J, TZKI M, ZIELASEK V, RISSE T, SCHMAL M, AND



- PARK C, FENTER PA, NAGY KL AND STURCHIO NC. 2006. Hydration and Distribution of Ions at the Mica-Water Interface. *Phys Rev Lett* 97: 016101- 1–4.
- PASSOS FB, ARANDA DAG AND SCHMAL M. 2000. The state of Tin on Pt-Sn/Nb₂O₅ catalysts. *Catal Today* 57: 283–289.
- REUEL RC AND BARTHOLOMEW CH. 1984. Effects of support and dispersion on the CO hydrogenation activity/selectivity properties of cobalt. *J Catal* 85: 78–88.
- RISSE T, CARLSSON A, BÄUMER M, KLÜNER T AND FREUND HJ. 2003. Using IR intensities as a probe for studying the surface chemical bond. *Surf Sci* 546: L829–L835.
- RISSE T, HILL T, MOZAFFARI-AFSHAR M, HAMANN H AND FREUND H-J. 2004. Structural Changes in Nanoparticle Catalysts as Monitored by their Magnetic Properties. *Angew Chem Intern Ed*, 43/4: 517–520.
- RISSE T, SHAIKHUTDINOV S, NILIUS N, STERRER M AND FREUND H-J. 2008. Gold Supported on Thin Oxide Films: From Single Atoms to Nanoparticles. *Acc Chem Res* 41: 949–956.
- ROSENIR RC, SILVA CM, SCHMAL M, FRET Y R AND DALMON JA. 1993. Effect of the support on the Fischer-Tropsch synthesis with Co/Nb₂O₅ catalysts. *J Chem Soc, Faraday Trans* 89: 3975–3980.
- SARKANY A, ZSOLDOS Z, STEFLER G, HIGHTOWER JW AND GUCZI L. 1995. Promoter Effect of Pd in Hydrogenation of 1,3-Butadiene over Co-Pd Catalysts. *J Catal* 157: 179–189.
- SATO K, IONOUE Y, KOJIMA I, MIYAZAKI E AND YASUMORI I. 1984. Infrared and X-ray photoelectron spectroscopy studies of carbon monoxide adsorbed on silica-supported cobalt catalysts. *J Chem Soc, Faraday Tran.* 1 80: 841–850.
- SCHANKE D, VADA S, BLEKKAN EA, HILMEN AM, HOFF A AND HOLMEN A. 1995. Study of Pt-Promoted Cobalt CO Hydrogenation Catalysts. *J Catal* 156: 85–95.
- SCHLÖGL R. 2008. Ammonia Synthesis. In: ERTL G, KNÖZINGER H, SCHÜTH F, WEITKAMP J (Eds), *Handbook of Heterogeneous Catalysis*, Wiley VCH Verlag: Weinheim 5: 2501–2575.
- SCHMAL M, ARANDA DAG, SOARES RR, NORONHA FB AND FRYDMAN A. 2000. A study of the promoting effect of noble metal addition on niobia and niobia alumina catalysts. *Catal Today* 57: 169–176.
- an Ultrathin Aluminum Oxide Film. *Phys Rev Lett* 97: 046101- 1–4.
- SHAIKHUTDINOV S ET AL. 2002. Interaction of oxygen with palladium deposited on a thin alumina film. *Surf Sci.* 501: 270–281.
- SIMON GH, KONIG T, NILIUS M, RUST H-P, HEYDE M AND FREUND H-J. 2008. Atomically resolved force microscopy images of complex surface unit cells: Ultrathin alumina film on NiAl(110). *Phys Rev B* 78: 113401- 1–4.
- STARR DE, MENDES FMT, MIDDEKE J, BLUM RP, NIEHUS H, LAHAV D, GUIMOND S, UHL A, KLUENER T AND SCHMAL M. 2005. Preparation and characterization of well-ordered, thin niobia films on a metal substrate. *Surf Sci* 599: 14–26.
- STERRER M, RISSE T, POZZONI UM, GIORDANO L, HEYDE M, RUST HP, PACCHIONI G AND FREUND H-J. 2007. Control of the Charge State of Metal Atoms on Thin MgO Films. *Phys Rev Lett* 98: 096107- 1–4.
- STRANICK MA, HOUALLA M AND HERCULES DM. 1987. Determination of the distribution of species in supported metal catalysts by X-ray photoelectron spectroscopy. *J Catal* 103: 151–159.
- TANABE K. 2003. Catalytic application of niobium compounds. *Catal Today* 78: 65–77.
- TUNG H-C, YEH C-T AND HONG C-T. 1990. Effects of cobalt loading on the properties of alumina-supported cobalt oxide. *J. Catal.* 122: 211–216.
- UHL A, SAINIO J, LAHTINEN J, SHAIKHUTDINOV S AND FREUND HJ. 2007. Preparation and structure of alumina supported niobia model catalysts. *Surf Sci* 601: 5605–5610.
- VAN’T BLIK HFJ AND PRINS R. 1986. Characterization of supported cobalt and cobalt-rhodium catalysts: I. Temperature-programmed reduction (TPR) and oxidation (TPO) of Co-Rh/Al₂O₃. *J Catal* 97: 188–199.
- WACHS IE. 2005. Recent conceptual advances in the catalysis science of mixed metal oxide catalytic materials. *Catal Today* 100: 79–94.
- ZECCHINA A, SCARANO D, BORDIGA S, RICCHIARDI G, SPOTO G AND GEOBALDO F. 1996. *Catal Today* 27: 403–435.
- ZIOLEK M. 2003. Niobium-containing catalysts – the state of the art. *Catal Today* 78: 47–64.
- ZSOLDOS Z, HOFFER T AND GUCZI L. 1991. Structure and catalytic activity of alumina supported platinum cobalt